Outer rise stress changes related to the subduction of the Juan Fernandez Ridge, central Chile

V. Clouard, J. Campos, A. Lemoine, A. Perez, E. Kausel

Outer rise stress changes related to the subduction of the Juan Fernandez Ridge, central Chile

V. Clouard,[1,2] J. Campos,[1,2] A. Lemoine,[1,3] A. Perez,[1,2] and E. Kausel[1,2]

Received 16 August 2005; revised 17 November 2006; accepted 13 December 2006; published 12 May 2007.

[1] Although outer rise seismicity is less common than interplate seismicity in subduction zones, a significant level of seismicity has occurred between the Nazca trench and Juan Fernandez Ridge, in central Chile, during the past 20 years. We first study the 9 April 2001 (Mw = 7.0) event and determine its focal mechanism, depth, and source time function by body-waveform inversion from teleseismic broadband data. The results indicate tensional faulting in the upper part of the mechanical lithosphere. Its strike (41°) is similar to those observed in events down dip of the slab at about 100 km depth, which could indicate that these earthquakes occur in preexisting structures formed at the trench. Compressive outer rise events have also occurred during the 1980s in front of the rupture zone of the 1985 Mw 7.8 Valparaíso Earthquake. To understand their relation with the state of stress of the lithosphere, we construct yield stress envelopes of the oceanic lithosphere, including static and dynamic stresses. Dynamic stresses are due either to slab pull, ridge push, resistive, and drag forces. We explain the sequence of compressive and tensional events by the accumulation of stress prior to 1985 when the subduction is assumed to be locked and after by the unlockage of the subduction by the Valparaíso interplate event. The yield stress envelope analysis enables us to quantify the accumulation of compressive forces before 1985 and the tensional force after.

Citation: Clouard, V., J. Campos, A. Lemoine, A. Perez, and E. Kausel (2007), Outer rise stress changes related to the subduction of the Juan Fernandez Ridge, central Chile, *J. Geophys. Res.*, *112*, B05305, doi:10.1029/2005JB003999.

1. Introduction

[2] Outer rise earthquakes are either normal or thrust events with tensional and compressional axes oriented approximately subhorizontally and perpendicular to the trench axis [*Christensen and Ruff*, 1988]. Tensional events are a standard feature of the subduction process as they occur at every major subduction zone. Shallow normal faulting outer rise events are associated with the bending of the plate [*Stauder*, 1968a, 1968b]. Studies of large tensional outer rise earthquakes showed these events can rupture nearly the entire oceanic lithosphere and are enhanced by the slab-pull effect of the downgoing slab [*Kanamori*, 1971; *Abe*, 1972]. Compressional events occur deeper than tensional ones [*Chapple and Forsyth*, 1979; *Seno and Gonzalez*, 1987; *Mueller et al.*, 1996b] and are rare in comparison to tensional ones (there is around one compressional event for six tensional ones, according to *Christensen and Ruff* [1988]).

[3] The spatial distribution of normal and compressive intraplate events within the subducting lithosphere is usually explained by plate bending models. These models [*Stauder*, 1968a, 1968b; *Chapple and Forsyth*, 1979; *Seno and Yamanaka*, 1996] predict tensional stress in the upper lithosphere, which agrees with the distribution of shallow normal faulting events, and a deeper compressional region, separated from the tensional region by a neutral plane. The average depth of the neutral plane is typically between 30 and 40 km [*Chapple and Forsyth*, 1979]. A statistical estimate of the depth limit between tensional and compressional zones within the subducting oceanic lithosphere indicates that the 450°C isotherm is a good proxy for the boundary [*Seno and Yamanaka*, 1996]. In addition to the plate bending, the temporal distribution of outer rise seismicity can be associated with stress accumulation and release during the seismic cycle [*Dmowska et al.*, 1988; *Taylor et al.*, 1996; *Dmowska et al.*, 1996]. In coupled regions, compressional earthquakes are triggered by the slow accumulation of bending and in-plane compressional stresses oceanward of the locked section, whereas tensional outer rise events generally follow large underthrusting events [*Christensen and Ruff*, 1983, 1988; *Astiz et al.*, 1988; *Dmowska et al.*, 1988; *Dmowska and Lovison*, 1988; *Lay et al.*, 1989].

[4] The occurrence of asperities along the thrust interface is expected to increase stress [*Dmowska and Lovison*, 1992; *Dmowska et al.*, 1996]. Asperities are areas marking the highest seismic moment release during large underthrusting events where stress and deformation rates during the earthquake cycle should be more pronounced. Outer rise

[1]Departamento de Geofísica, Universidad de Chile, Santiago, Chile.
[2]Also at Laboratorio Internacional Asociado Montessus de Ballore CNRS-IPGP-ENS/Universidad de Chile, Santiago, Chile.
[3]Now at Development Planning and Natural Risks Division, Bureau de Recherches Géologiques et Miniéres, Orléans, France.

0148-0227/07/2005JB003999$09.00

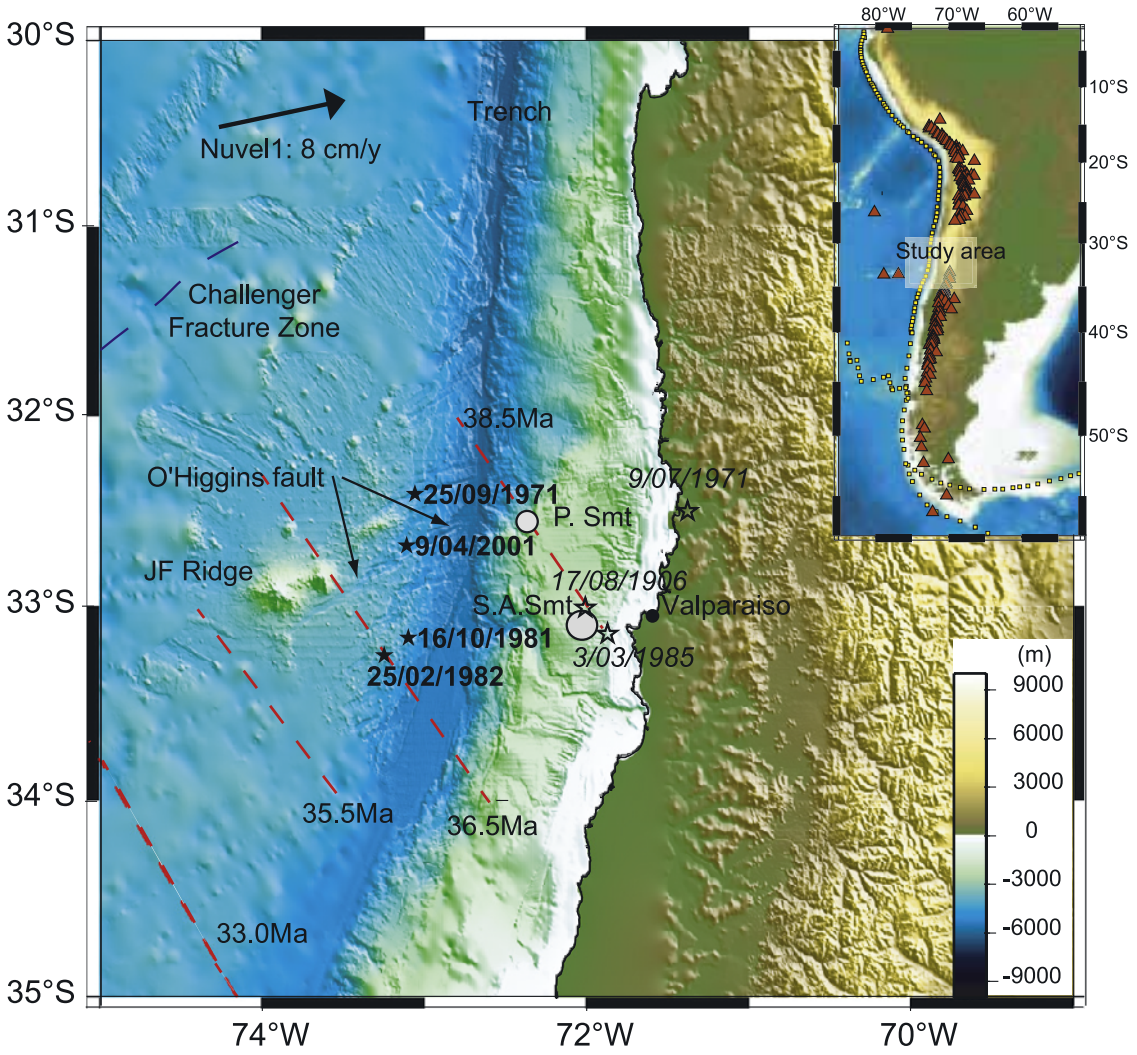

Figure 1. Bathymetric map of the studied area. Red dashed lines represent the main magnetic anomalies [*Müller et al.*, 1996; *Yáñez et al.*, 2001]. Relative convergence velocity of Nazca Plate with South America is from NUVEL-1 [*DeMets et al.*, 1990]. Black stars indicate the epicentral locations of main outer rise events (April 2001, 1971, 1981, and 1982). Open stars represent 1906, 1971, and 1985 interplate earthquakes. Gray disks with black outline represent subducted seamounts (P. Smt: Papudo seamount, S.A. Smt: San Antonio seamount). The upper right insert shows the south American continent and the study area. Red triangles represent recent active volcanoes and the dotted yellow lines the plate boundaries.

and in-slab intermediate depth events tend to lie within corridors through thrust zone asperities and parallel to the direction of convergence.

[5] The depth of these earthquakes reflects the state of stress of the lithosphere according to its rheological properties. Rheological models deduced from laboratory data were proposed during the 1980s [*Goetze and Evans*, 1979; *Brace and Kohlstedt*, 1980; *Kirby*, 1980]. In the shallower part of the lithosphere, strength is governed by frictional sliding along preexisting faults, and in its deeper part, the lithosphere undergoes plastic flow. Between these two regions, a brittle-ductile transition zone exists. Maximum rock strength plotted versus depth provides stress envelopes, which represent the stress limit that the lithosphere can support without brittle or plastic flow deformation. Obviously, earthquakes can nucleate only in the brittle or semibrittle area. Their type (compressive or tensional) depends on the loading history of the plate. *McNutt and Menard* [1982] and *Mueller et al.* [1996a, 1996b] calculated yield strength envelopes for oceanic lithosphere in outer rise areas, in the contexts of bending, unbending, slab-push or slab pull, or in the case of a more complex sequence (e.g., bending followed by slab-pull). We use this method to constrain the state of stress of the oceanic lithosphere with the a priori information of outer rise seismic events.

[6] Our goal is to estimate the state of stress of the oceanic lithosphere in the central Chile outer rise area and its evolution between two sequences of outer rise earthquakes. The first step is the detailed study of the 9 April 2001 outer rise earthquake (see location, Figure 1) and its associated aftershocks. Next, a geometrical approach is used to define the shape of the bending lithosphere, which then

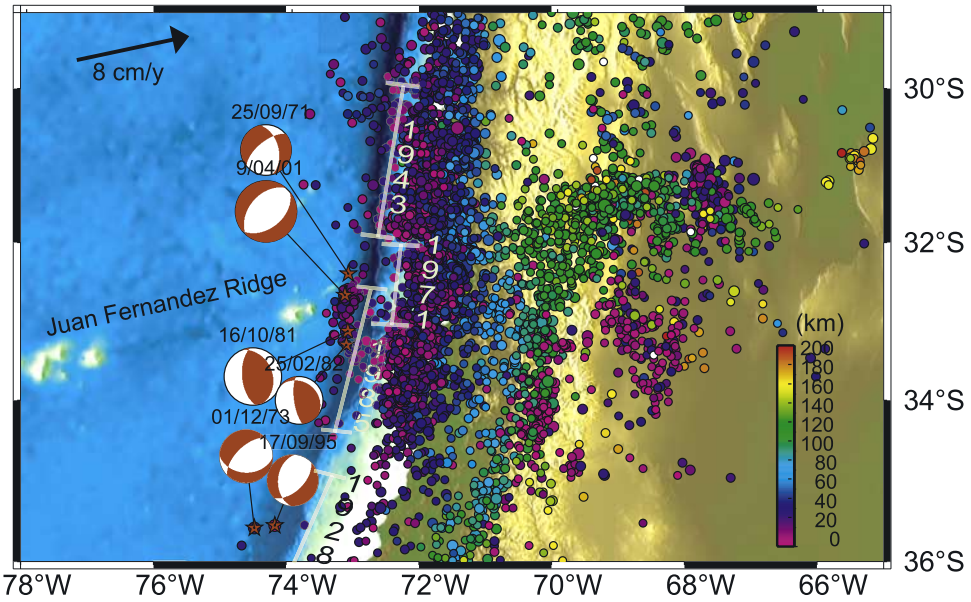

Figure 2. Seismicity (Mw > 4) associated with subduction landward of the study area, from NEIC Catalogue between 1973 and 2003. Color scale according to the event depth. White lines represent the rupture lengths of underthrusting earthquakes (adapted from *Comte et al.* [1986]). Mechanisms and locations of main outer rise events are shown.

allows yield strength envelopes to be estimated. The final analysis of the stress state and strength of the oceanic lithosphere includes an examination of large earthquakes that occurred in the study area during the last 30 years.

2. Tectonic Setting

[7] The study area (Figure 1) corresponds to the eastern part of the Nazca plate, from 30°S to 35°S. The age of the oceanic lithosphere in the study area ranges from 33 Ma in the southwest to 38 Ma in the northeast [*Cande and Herron*, 1982; *Yáñez et al.*, 2001]. All this seafloor was formed at the Pacific/Farallon Ridge. Plate convergence velocities in our study area deduced from NUVEL-1 [*DeMets et al.*, 1990] are 80 mm/year along a N78.1° strike, and from GPS data [*Kendrick et al.*, 2003] are 63.2 mm/year along a N79.5° strike. Despite the difference in rate, only the direction of convergence is relevant in our study and both sources are in agreement. We use the N78.1° direction.

[8] The main tectonic feature in the study area is the Juan Fernandez (JF) Ridge (Figure 1). In this region the JF Ridge comprises a guyot (8.5 ± 0.4 Ma, J.M. O'Connor, manuscript in preparation, 2005) and a seamount, which form the O'Higgins Seamounts. This is the eastern part of a hotspot chain. The present-day location of the JF hotspot would be to the west of Juan Fernandez Islands [*von Huene et al.*, 1997]. The Chilean trench between the Nazca and South America plates reaches 6200 m-depth to the north of the JF Ridge and is partially buried by sediments to the south. The JF Ridge appears to act as a barrier to sediment transport from the south to the north [*Lawrie and Hey*, 1981]. Parallel to the JF Ridge, to the north and to the south, are unusually long (ca. 100 km) horst-and-graben type faults, whose scarps in the southern area reach about 1000 m-high near the trench axis [*von Huene et al.*, 1997]. The main one, the O'Higgins fault, is indicated in Figure 1.

[9] Along the Andean margin, the subducted slab is morphologically segmented into steep subduction and flat-slab subduction regions [*Barazangi and Isacks*, 1976]. Flat-slab areas are revealed by the shape of the Wadati-Benioff zone deduced from seismic data [*Engdahl et al.*, 1998] and tomographic images from a global travel time tomographic model [*Bijwaard et al.*, 1998]. Two areas are subject to flat-slab subduction along the Andean trench [*Barazangi and Isacks*, 1976]: central Chile (between 27° and 33°S) and central Peru. Central Chile is characterized by a 15° dip angle to depths of ~100 km and then by subhorizontal slab for several hundreds of kilometers [*Hasegawa and Sacks*, 1981].

[10] The seismic energy released during earthquakes within the upper plate is 5 to 10 times greater in the Central Andes flat-slab area than in adjacent north and south segments [*Gutscher*, 2002], which implies a higher degree of interplate coupling. It is consistent with a longer contact area and cooler temperatures [*Gutscher*, 2002]. To the east of our study area, stress tensors were determined for the interplate coupled zone: at shallow depths (0 to 70 km), the slab is under compression due to plate convergence with some normal faulting events in the oceanic plate, whereas far from the trench, at intermediate depths, the slab is under tension due to the slab pull [*Pardo et al.*, 2002].

3. Seismic Analysis

3.1. Seismicity of Valparaíso Area

[11] The study area is located at the transition from flat subduction, northward, to normal subduction, southward [*Barazangi and Isacks*, 1976]. Around the subduction of JF ridge a high level of seismicity occurs from superficial to intermediate depths. Figure 2 shows that on a 150 km wide band along the trend of JF ridge, seismicity associated with subduction is particularly intense. In this area the most

Table 1. Main Outer Rise Earthquakes Registered Off Coast of Valparaíso

Date	Latitude, Longitude	Depth	Magnitude	Strike, Dip, Slip
09/25/1971[a]	−32.4°, −73.06°	4 km (*ISC*)	M_s = 5.8	231, 64, −46[b]
12/01/1973[a]	−35.59°, −74.48°[d]	23 km (*ISC*)	M_s = 5.9	226, 61, −116
16/10/1981[a]	−33.13°, −73.07°[d]	30 km	M_s = 7.2	175, 59, 99
02/25/1982[a]	−33.3°, −73.09°[d]	27 km (*ISC*)	m_b = 5.2	172, 72, 107
09/17/1995[c]	−35.56°, −74.17°[d]	15 km	M_w = 5.6	184, 42, −124
04/09/2001[e]	−32.84°, −73.32°	12 km	M_w = 7	41, 44, −84

[a]Source is *Korrat and Madariaga* [1986].
[b]Parameters may not by well constrained.
[c]Source is CMT Harvard.
[d]Source is NEIC.
[e]Source is this study.

recent great interplate earthquakes (Figures 1 and 2) are the 1985 Valparaíso M_w = 8 and the 1971 M_s = 7.5 events [*Mendoza et al.*, 1994; *Malgrange et al.*, 1981]. The aftershock areas of these two earthquakes overlap between 32°.5 and 33°S [*Comte et al.*, 1986], which correspond to the latitude of the 9 April 2001 event (Figure 2). Here, outer rise earthquakes are less common than earthquakes occurring at the coupled interface between subducting plate and continental plate. However, the region seaward of Valparaíso experienced six large events from 1971 to 2001 (Table 1), of which the last is the 9 April 2001 earthquake on which our study focuses.

[12] Outer rise seismicity since 1973 for this area can be divided into two sequences: the first began with the 16 October 1981 M_s = 7.2 event, which occurred south of JF Ridge at a depth of 30 km [*Korrat and Madariaga*, 1986]. Its focal mechanism indicates compression within the oceanic plate (Figure 2). It was followed by the 25 February 1982 earthquake (m_b = 5.2, z = 27 km, Table 1). Its focal mechanism was very similar to that of the 1981 event, showing compression parallel to the axis of JF Ridge (Figure 2). The second sequence of outer rise seismicity was associated with 9 April 2001 earthquake (M_w = 7.0), which is studied in detail in this paper. This event was followed by a high level of microseismicity that is still active to date. This earthquake occurred very close to the epicenter of the 25 September 1971 event (m_b = 5.5, z = 4 km, Table 1), which showed extension perpendicular to trench axis (Figure 2). Two outer rise events of the same kind occurred around latitude 35.5°S on 1 December 1973 (m_b = 5.8, z = 23 km) and on 17 September 1995 (m_b = 5.9, z = 7 km). They both indicate extension, perpendicular to the trench axis for the 1995 one, and subparallel to Nazca-South America relative plate motion and to the JF Ridge for the 1973 one (Figure 2).

3.2. Event of 9 April 2001

[13] The 9 April 2001 earthquake occurred between the O'Higgins seamounts and the Chile trench, in an area fractured by horst-and-graben type faults (Figure 1). It was the second biggest outer rise event recorded close to Juan Fernandez ridge (see Table 1). The fault plane solution reported by Harvard Centroid Moment Tensor (CMT) Catalogue (Table 2) is a normal faulting mechanism at 15 km depth and dipping at 46°, but the strike of 33° is not parallel to the trend of the trench in this area. Body wave analysis will confirm this result and allows us to propose a complex source-time model for the rupture of this event.

[14] For the body wave study we used more than 50 VBB teleseismic digital records from the Incorporated Research Institutions for Seismology (IRIS) network. Only mantle body waves from stations at distances of $30° \leq \Delta_P \leq 90°$ and $34° \leq \Delta_{SH} \leq 87°$ are included in our data set in order to avoid upper mantle and core arrivals. Twenty-nine P waves and thirty SH waves are selected in order to obtain a good azimuthal distribution of stations around the epicenter (Figure 3). For inversion of the body wave data we use the procedure proposed by *Nábělek* [1984]. In this method we invert for multiple sources and solve simultaneously for focal mechanism, centroid depth, and source-time function for subevent. In order to get the best estimate of the source parameters, we minimize the residuals between the observed and theoretical seismograms and the difference between the parameters of the a priori and the best fit model. The objective functional for the inversion was chosen as the following $\mathcal{L}^2$ norm

$$\mathcal{L}^2 = [d - m(p)]^T C_{d_0}^{-1} [d - m(p)] + (p - p_0)^T C_{p_0}^{-1} (p - p_0) \quad (1)$$

where d is the vector of observed seismograms, m the corresponding synthetic seismograms, p the estimated model parameters, p_0 an a priori estimate of the model, and C_{d0} and C_{p0} are the a priori estimates of the variance of the data and model parameters, respectively.

[15] We follow the same procedure applied by *Campos et al.* [1994], who did a limited exploration of the parameter space. In order to control the resolution of the inversion, a stepwise procedure is carried out, increasing the model complexity at each new inversion. We focused our interest on rupture propagation, on possible focal mechanism variation, and on the subevent distribution. To estimate the goodness of fit of the models, we use the same normalized residual that *Campos et al.* [1994] used. The velocity and density distribution adopted in the source region comes from *Kopp et al.* [2004]. Anelastic attenuation along the propagation path was parametrized using an effective atten-

Table 2. Fault Plane Solution

Moment Tensor	Harward CMT	This Study
Mo, Nm	1.17×10^{19}	4.6×10^{19}
Strike	33°	41°
Dip	46°	44°
Rake	−86°	−84°
H, km	15	12
Mw	6.6	7.0

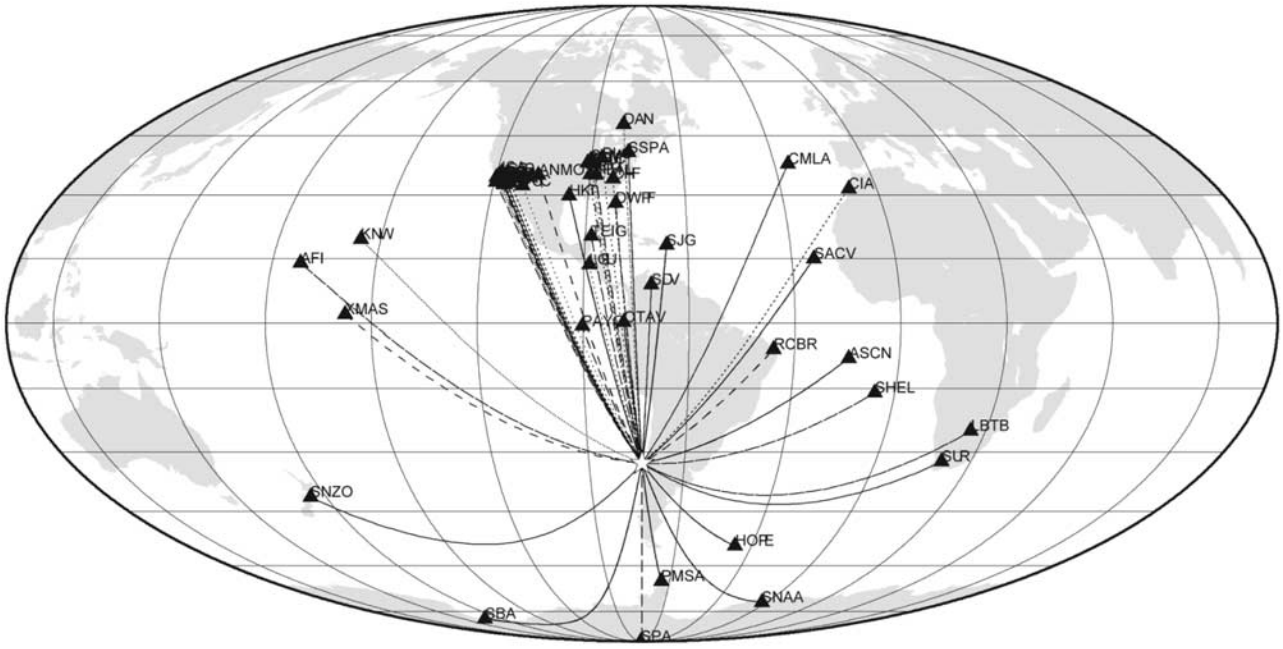

Figure 3. Azimuthal coverage of teleseismic stations (black triangles) used in the body wave inversion. Black lines: P and SH waves; dotted lines: SH waves; dashed lines: P waves.

uation t^* of 1 s for P waves and a t^* of 4 s for SH waves. All the observed records are equalized to displacement seismograms with the same gain at a distance of 40° from the epicenter. In order to avoid problems with low- and high-frequency noise due to the integration procedure, displacement records are filtered with a band-pass filter (Butterworth of order 3) between 0.01 and 1 Hz. Because SH wave amplitudes are much larger than P wave amplitudes and because the sensitivity of the least squares inversion is directly proportional to the power of the signal, we apply a weighting to give the same significance to both types of waves. The total RMS misfit is defined as the sum of the P and SH normalized residuals divided by the root square of the total normalized variance of the data.

[16] The best point source model consistent with P and SH waves is determined from the body wave inversion. From this model we determine the depth of the source centroid and the orientation of the fault plane. The inversion process is started using the a priori model of the CMT solution obtained by Harvard (Table 2) and a source-time function parametrized by a sequence of isosceles triangles of rise time 1 s and variable amplitude for a total duration of 50 s. From linearized inversion we obtain a strike of 41°, a dip of 44° and rake of −84° (Table 2). We also find the depth of source centroid to be 12 km and the seismic moment to be $Mo = 4.6 \times 10^{19}$ Nm.

[17] The waveform fits are quite good (Figures 4 and 5). Hence the point source model explains the complex body wave signals reasonably well. The focal mechanism is well constrained as can be seen from the amplitude variation of P and SH waves with azimuth (Figures 4 and 5). In particular, SH waves for stations SJG and SACV show a clear polarity change when crossing the nodal plane.

[18] Directivity effects can be seen in Figure 4: the vertical arrows show the widening of the P wave pulses from north to south, indicating a rupture propagation to the north. This SW to NE directivity source effect is in good agreement with the 4 day aftershock distribution (Figure 6), further confirming that the strike of the focal plane is parallel to JF Ridge. The source-time function is a complex sequence consisting of three main pulses totaling 40 s source duration. This result agrees with the direction of rupture propagation starting at the southwest of the aftershocks area.

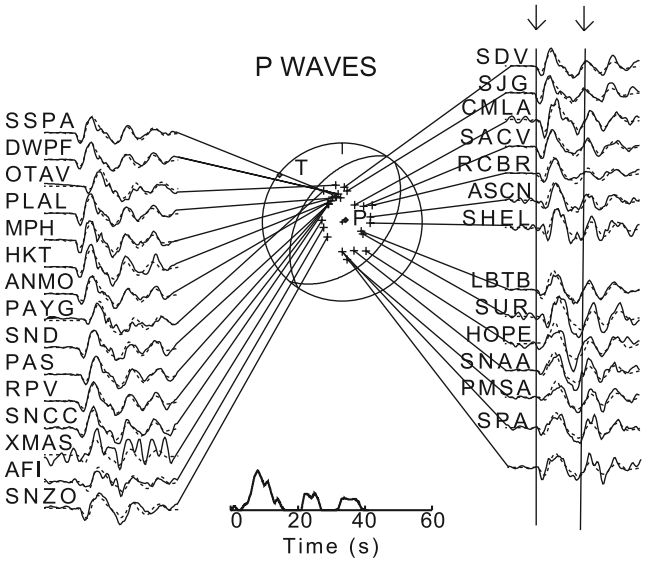

Figure 4. Point source modeling of P waveforms of the Mw = 7.0 9 April 2001 event, off coast of Valparaíso. Depth was 12 km. Solid and dashed lines represent observed and synthetics displacement, respectively. Source time function had a duration of 40 s.

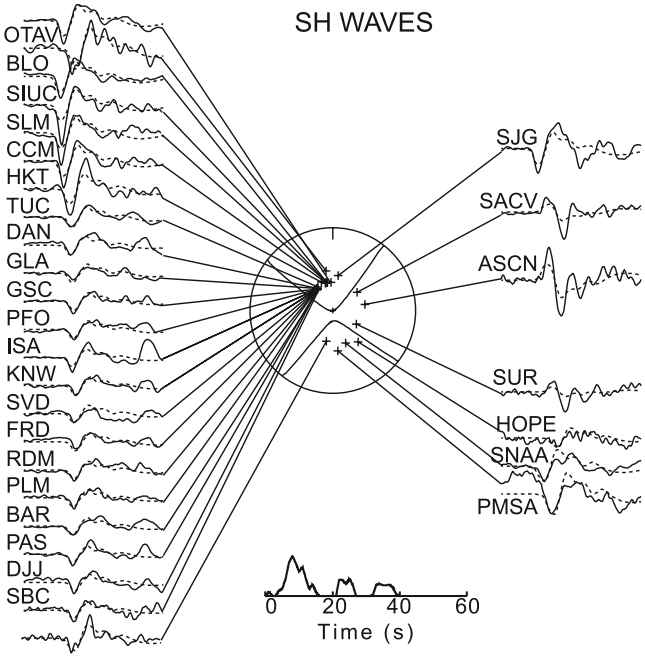

Figure 5. Point source modeling of SH waveforms of the Mw = 7.0, 9 April 2001 event. Legend as in Figure 4.

3.3. Aftershock Seismicity

[19] The outer rise seismic data used are those recorded by the Seismological Service of Chile University (GUC), with a permanent local network (see location Figure 6). This network comprises 21 stations between 32°S and 35°N including accelerometers, broadband stations, and short periods 1 and 3 components. From 9 April 2001 to 28 February 2003, a total of 220 events were recorded. A database is generated, which includes the digital seismograms obtained for each of the 220 events. The readings of either P and S wave arrivals are made for each event using the SEISAN package [*Havskov and Ottemoller*, 1999] to obtain the initial hypocenter locations. The final hypocenter relocations are made using the HypoDD program [*Waldhauser*, 2001]. The 9 April 2001 main shock is relocated at 32.84°S and 73.32°W (Figure 6).

[20] We studied aftershocks occurring during a period of 52 days after the principal event of 9 April 2001. A total of 130 aftershocks were recorded, including 72 (55%) during the first 4 days (Figure 7). We consider this important seismic activity of the first 4 days as the actual aftershock activity, and thus only these events are kept in the following analysis. The final relocation of the mainshock and of these 72 aftershocks is shown in Figures 6 and 8. Earthquakes are concentrated in a cluster located 50 km west of the trench to the northeast of the main shock epicenter. Because of the on-land location of our local network, the location of the aftershocks are systematically shifted to the east of the main shock, whose location was obtained using a world coverage of seismic stations. The aftershock depth distribution within the oceanic lithosphere ranges from 16 to 46 km (error ≈5 km), and their magnitudes from 3.4 to 4.4. With the method described above, the hypocenter depth of the main event is 18.4 km (error ≈5 km), in agreement with NEIC catalogue solution and with our previous result of the centroid depth of 12 km. We tried to compute focal mechanisms for the largest magnitude aftershocks to better understand fault mechanism at depth and the relation between these events and the main event. Unfortunately, owing to the location of the local network, which is only on-land eastward of the seismic cluster, no convincing solution was produced.

[21] However, together with the modeling of the 9 April 2001 event, the 4 day aftershock distribution confirms that

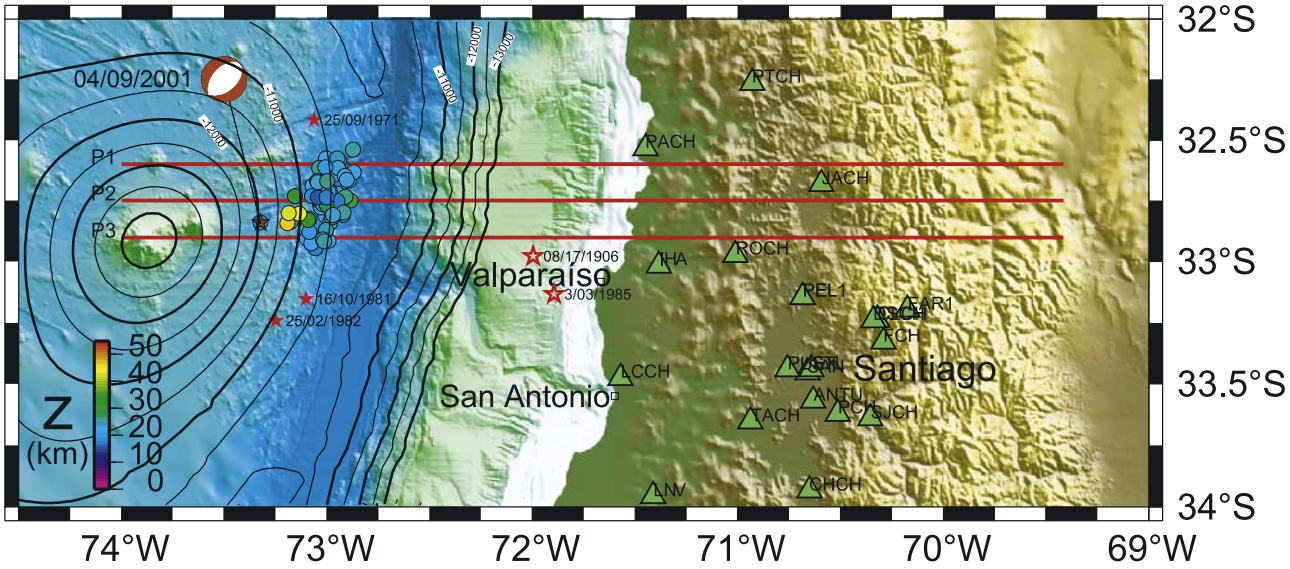

Figure 6. Location of 9 April 2001 2 week aftershocks over detailed bathymetry: colored circle according to their depth. Red stars correspond to outer rise events and open stars to interplate earthquakes. Tracks of the Figure 8 profiles are the red lines. Isocontours of the Moho depth are shown. Green triangles are the local seismic stations used to locate aftershocks.

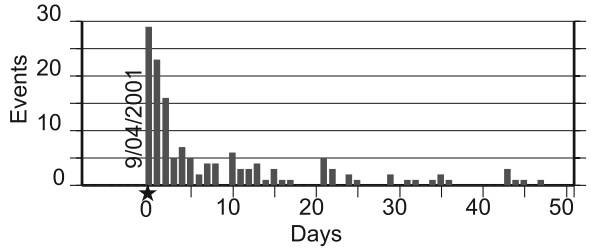

Figure 7. Histogram of local outer rise seismicity before and after 9 April 2001 earthquake, from 1 April to 30 May 2001.

the strike of the focal plane is not parallel to the main trench strike but is in fact subparallel to the JF Ridge and the O'Higgins fault.

4. Characterization of the Oceanic Lithosphere

[22] Deformation of the lithosphere in the study area, associated with a realistic rheology of the oceanic lithosphere, can be used to deduce the lithospheric stress distribution [*Goetze and Evans*, 1979; *McNutt and Menard*, 1982]. We first determine the shape of the lithosphere assuming an elastic behavior. We assume that deformation is produced by two phenomena: first, the bending of the lithosphere prior to subduction, and second, the deflection of the lithosphere under the JF Ridge volcanic load. The characteristics of the bending of the lithosphere prior to subduction can be directly determined from the bathymetry near the rise. This provides the deformation of the lithosphere due to the subduction, the elastic thickness, and the curvature of the dipping lithosphere. The elastic thickness is used to determine the flexure of the crust under the JF seamounts to define the shape of the upper oceanic lithosphere. The curvature is used to compute the yield strength envelope. This complete characterization of the oceanic lithosphere enables us to carry out the analysis of the outer rise seismicity in our study area.

4.1. Bending Due to Subduction

[23] The bending of the lithosphere prior to the subduction induces considerable flexure [e.g., *Turcotte and Schubert*, 1982; *Watts et al.*, 1995]. This bending is commonly modeled in two dimensions by a universal deflection profile deduced from elastic plate theory [*Caldwell et al.*, 1976]. With the proper boundary conditions, the value of the flexure, w, along a profile perpendicular to the trench can be expressed by

$$w = w_b\sqrt{2}\sin\frac{\pi x}{4x_b}\exp\frac{\pi(x_b - x)}{4x_b} \tag{2}$$

where w_b is the magnitude of maximum positive deflection, at coordinate x_b, the distance from the point at the trench where the plunging lithosphere reaches the regional value of the bathymetry (see Figure 9). Local values for w_b and x_b are deduced from bathymetric data. The most recent bathymetric synthesis including multibeam data [*Zapata*, 2001; *Clouard et al.*, 2003] is used to realize a modal analysis. First, we made the age correction of the bathymetric data using the subsidence model of *Parsons and Sclater* [1977]

$$depth(t) = 2500 + 350\sqrt{t} \quad t \text{ in Ma}. \tag{3}$$

[24] Then all the data are projected along tracks perpendicular to the trench and spaced by 1′, which is greater than the accuracy of bathymetric data. The distance of each depth point to the trench is calculated so that the deepest point of each profile is at distance 0. We construct a grid where the depth is a function of the distance to the trench, and z is the number of points in each cell (Figure 9). This representation was proposed by *Renkin and Sclater* [1988] to select the mode (the most common value in a population of numbers) of depth as a function of distance. It avoids the biasing that could occur if we had constructed our analysis only with a few bathymetric profiles, where the effect of seamounts could be predominant. A mode profile is deduced from the maximum of the grid at each distance step. The universal profile is then computed by finding the optimal value of the parameters w_b and x_b that minimize the misfit between the modal and the predicted profile, using the misfit formula of *Levitt and Sandwell* [1995]. We find w_b = 325 m and x_b = 35 km for a misfit value of 0.53 m. Shifted by 6 km below the depth of the regional seafloor, the universal profile then also can represent a typical profile of the Moho in the study area. To completely define the effective shape of the Moho, we also have to take into account its deflection under JF Ridge load.

4.2. Flexure Under Juan Fernandez Ridge Loading

[25] To compute the deflection of the lithosphere under JF Ridge loading, the value of the elastic thickness of the lithosphere can be deduced from its bending characteristics. The distance x_b is directly related to α, the flexural parameter by $x_b = \frac{\pi\alpha}{4}$, with $\alpha = [\frac{4D}{(\rho_m\rho_w)g}]^{1/4}$ [*Caldwell et al.*, 1976]. T_e, the elastic thickness is related to D, the flexural rigidity of the lithosphere, by $D = \frac{ET_e^3}{12(1-\nu^2)}$, where E is the Young's modulus, and ν the Poisson's ratio. With x_b = 35 km, the elastic thickness of the lithosphere is 15.3 km. We use the numerical approach developed by *Watts et al.* [1975] to solve in three dimensions the equation that governs w

$$D\nabla^4 w + (\rho_m - \rho_l)gw = q(x,y) \tag{4}$$

where ρ_l is the load density, ρ_m is the mantle density, ∇^4 is the biharmonic operator, $q(x, y)$ is the vertical load derived from the bathymetric grid, and g is the acceleration due to gravity. Density values and other parameters are shown Table 3. The deepest deflection is 2 km under O'Higgins guyot, in good agreement with values deduced from seismic refraction [*Kopp et al.*, 2004].

[26] Finally, a grid is constructed from the one obtained from the deflection of the seafloor under the JF Ridge, to which the universal profile is added. This represents the total deformation of the upper lithosphere (Figure 6) and reflects the shape of the Moho and the upper lithosphere without "noise" such as seamounts or faults. Note that the 9 April 2001 earthquake did not occur at the top of the

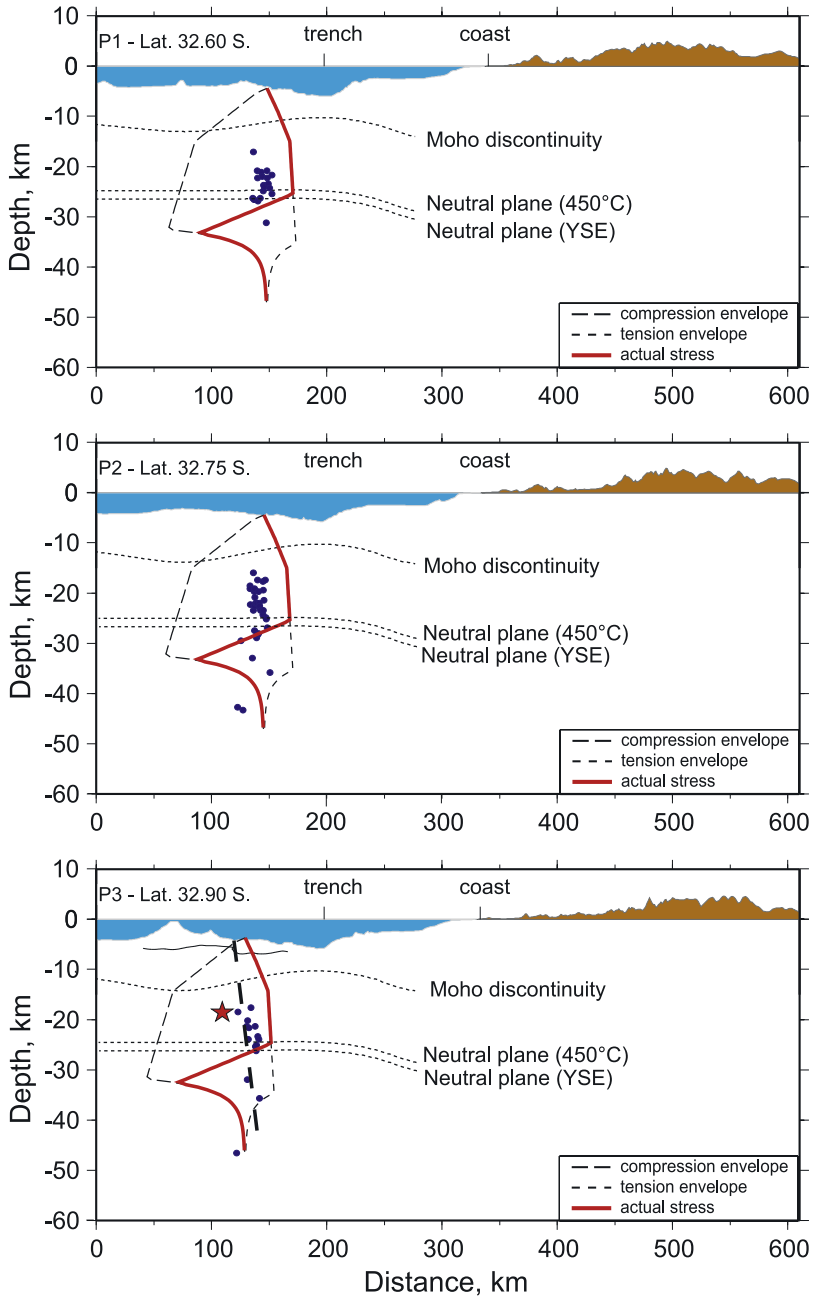

Figure 8. Vertical cross-sections of the lithosphere along profiles P1 (top), P2 (middle) and P3 (bottom), perpendicular to the trench (see location on Figure 6). The shape of the Moho derives from the deflection of the lithosphere due to subduction and the JF load. The depth of the 450° isotherm is based on the cooling plate model of *Parsons and Sclater* [1977]. The depth of the neutral plane deduced from the Yield Stress Envelope (YSE) comes from Figure 10. Black dots represent the 9 April 2001 aftershocks, and the main event is represented by a star. On profile P3, the limit of the upper crust obtained by seismic refraction [*Kopp et al.*, 2004] is the thin line. A possible fault plane is drawn in heavy dashed line from the seafloor JF fault, through the fault seen in the upper crust.

bending lithosphere (Figure 6), as might have been the case if the bending was the unique stress factor. The epicenter of our main event is shifted to the west of the trench because of the perturbation produced in the stress field by the JF Ridge.

4.3. Construction of the Yield Strength Envelope

[27] An elastic lithosphere model is appropriate to describe lithospheric deformation when stress is not too high, as, for example, when isolated volcanoes load the seafloor or the lithosphere bends prior to subduction. The elastic model approximates the complex rheology of brittle failure in the upper lithosphere and ductile creep below, down to a depth corresponding to the mechanical thickness of the lithosphere. However, to understand how stress is distributed in the lithosphere, we use the Yield Strength Envelope (YSE) [*Goetze and Evans*, 1979; *Kirby*, 1980;

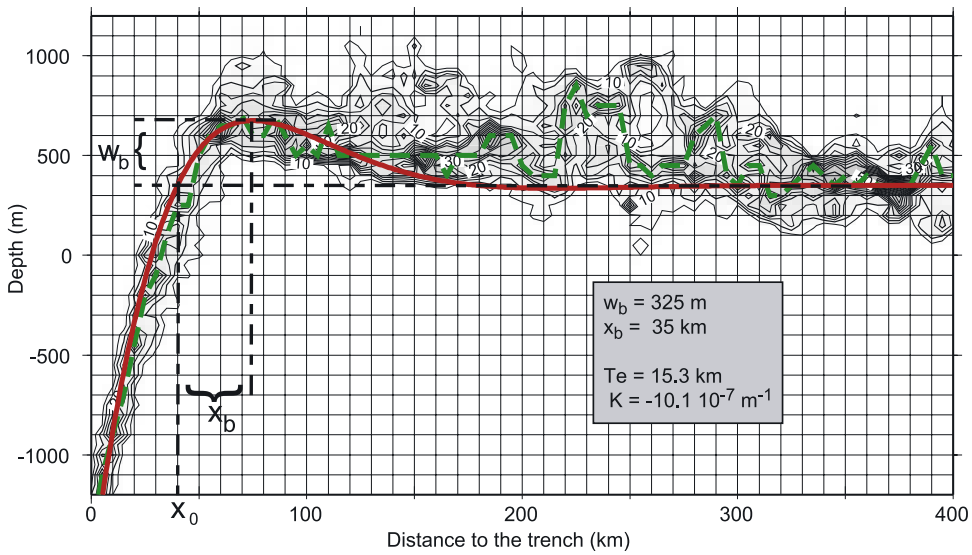

Figure 9. Determination of the universal profile of the deflection of the lithosphere prior to subduction: Modal representation of bathymetric data between 31.9° and 32.9°S and 72° to 75°W with age correction. Depth points are extracted from profiles spaced by 1′, perpendicular to the trench. Origin of the profiles (x = 0) is taken at the lowest point assumed to represent the trench. The origin of the y-axis corresponds to the normal depth according to the age of the lithosphere. Dashed thick line passes through the maxima of the modes, and best fit with the universal profile (thick line) provides x_b = 35 km and w_b = 325 m.

Bodine et al., 1981]. Stress envelopes are profiles of maximum rock strength plotted versus depth. They are derived from laboratory experiments on real rocks. Deformation in the upper brittle lithosphere is governed by frictional sliding and described by linear equations deduced from Byerlee's law [*Byerlee*, 1978] and deeper and until the bottom of the mechanical lithosphere, the plastic flow strength of the rocks is approximated by power law creep equations.

4.3.1. Reference YSE

[28] The depth of the mechanical lithosphere is usually assumed to lie between the 600 and 800°C isotherm [*Scholz*, 2002] and was found to be at the depth of the 800°C isotherm in our study area [*Judge and McNutt*, 1991]. This isotherm corresponds to a value of 41.5 km below the seafloor and hence lies about 45.5 km below sea level. To construct the brittle and the ductile parts of our reference YSE, we adopt the coefficients proposed by *Mueller et al.* [1996a], in the case where the stress is reduced by the pore pressure and where presence of water is assumed. In the brittle zone, the constitutive equations of the strength limit, $\Delta\sigma$, are given by

$$\begin{aligned} \Delta\sigma &= 3.68\sigma_{zz} && \sigma_{zz} \le 22\ MPa \\ \Delta\sigma &= 2.12\sigma_{zz} + 35\ MPa && \sigma_{zz} \ge 22\ MPa \end{aligned} \tag{5}$$

for compression and by

$$\begin{aligned} \Delta\sigma &= 0.79\sigma_{zz} && \sigma_{zz} \le 100\ MPa \\ \Delta\sigma &= 0.68\sigma_{zz} + 11\ MPa && \sigma_{zz} \ge 100\ MPa \end{aligned} \tag{6}$$

for tension, where $\sigma_{zz} = \Delta\rho gz$ is the lithostatic pressure. At higher temperature, the dominant mechanism for failure is ductile flow and is represented by a power law relationship between the yield strength $\Delta\sigma$ and the strain rate $\dot{\epsilon}$ [*Goetze*, 1978]

$$\Delta\sigma = \left[\frac{\dot{\epsilon}}{B}\exp\left(\frac{Q}{RT}\right)\right]^{1/n} \tag{7}$$

where Q is the activation energy, T is the temperature, R is the universal gas constant, and B and n are constants that depend on the material. In our case we use the values of wet dunite [*Chopra and Paterson*, 1981]. We assume a linear variation of T with depth, $T(°K) = 273 + \alpha z$. Here α is calculated between 0 and 80 km, the depth of the bottom of a 38 Ma lithosphere and for a temperature of the asthenosphere of 1573°K. The strain rate depends on the duration of the load or, in our case, on the changes in the plate curvature. In outer rise context, a common value is 10^{-15} s^{-1} [*Bodine et al.*, 1981; *Mueller et al.*, 1996a]. Values of parameters and constants used in the construction of the YSE are reported Table 4.

Table 3. Values of Parameters and Constants Used in Flexural and Gravity Modeling

Name	Symbol	Value	Unit
Young's modulus	E	1.0×10^{11}	Pa
Poisson's ratio	ν	0.25	
Acceleration due to gravity	g	9.81	m s^{-2}
Newton's gravitational constant	γ	6.67×10^{-11}	m^3 kg^{-1} s^{-2}
Load density	ρ_l	2700	kg m^{-3}
Water density	ρ_w	1030	kg m^{-3}
Mantle density	ρ_m	3350	kg m^{-3}

Table 4. Parameters and Constants Used to Construct the YSE

Name	Symbol	Value	Unit
Density contrast between the plate and the water	$\Delta\rho$	2300	kg m^{-3}
Strain rate	$\dot{\epsilon}$	10^{-15}	s^{-1}
B wet dunite	B	7.58×10^{-17}	Pa^{-n} s^{-1}
Q activation energy for wet dunite	Q	4.44×10^{5}	J mol^{-1}
n power law exponent for wet dunite	n	3.4	
Universal gas constant	R	8.314	J K^{-1} mol^{-1}
Temperature gradient	α	1.96×10^{-2}	K m^{-1}

[29] Between the purely brittle or ductile regimes, both processes can occur, but constitutive equations of the brittle-ductile transition zone are not well constrained (see discussion in the work of *Kohlstedt et al.* [1995]). This is of particular interest in our study, as most of the studied earthquakes occurred in this zone, and as the bottom of the seismogenic zone cannot be deeper than the top of the ductile zone [e.g., *Scholz*, 2002]. Following *Kohlstedt et al.* [1995], we construct a linear curve from 10 km depth (the end of purely brittle behavior) to the depth where the stress necessary for plastic flow equals the effective confining pressure, $\sigma_1 - \sigma_3$. In tension, $\sigma_1 = \sigma_{zz}$ and $\sigma_3 = \Delta\sigma$ and in compression, $\sigma_1 = \Delta\sigma$ and $\sigma_3 = \sigma_{zz}$, which leads to the intersection point between ductile and semibrittle curves at 30.5 km in compression and 33.5 km in tension. The final YSE is represented Figure 10. The highest value of the reference YSE is 202 MPa in tension and 704 MPa in compression. They are in the range of other YSEs [e.g., *Mueller et al.*, 1996a]. In the next paragraph our analysis of the dynamical force within the lithosphere will be bound by these values.

4.3.2. Static and Dynamic Stress of the YSE

[30] To compute the actual stress distribution within the lithosphere, we assume that stresses are a combination of (1) thermal stress, (2) the plate bending stress prior to subduction, and (3) an in-plane tensional stress as indicated by the focal mechanism of the 9 April 2001 event.

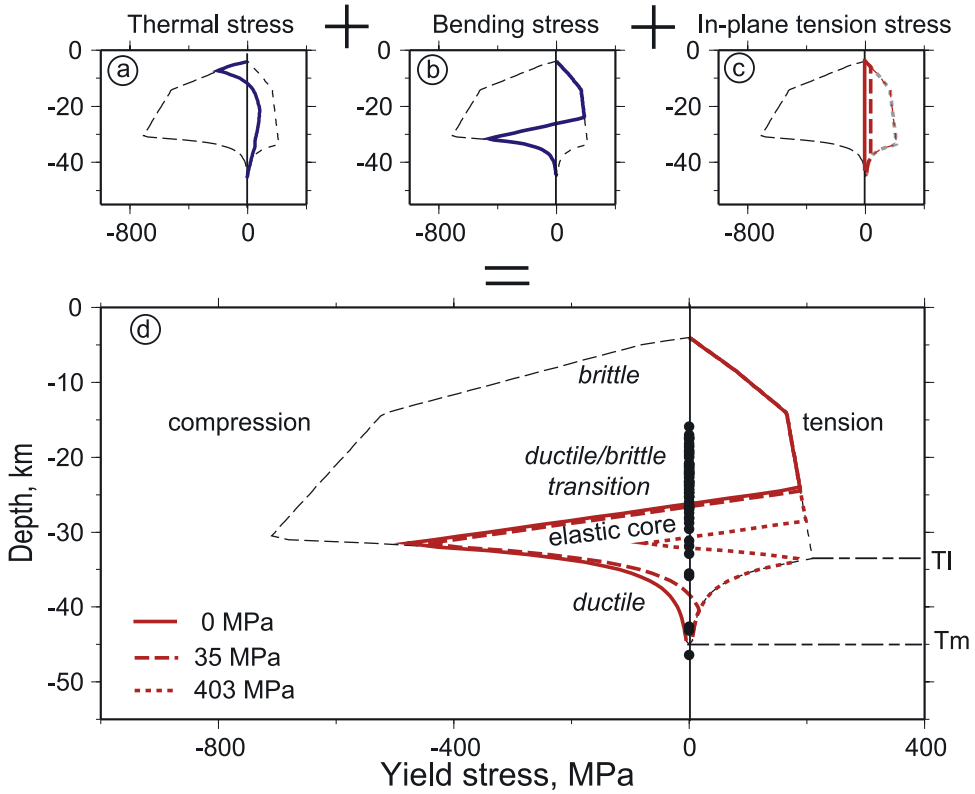

Figure 10. YSE computed in the case of (a) pure thermal stress, (b) pure bending, and (c) pure tension, and (d) their sum with thermal and bending preceding tension. Tension (right part of the figures) corresponds to positive stresses, and compression corresponds to negative ones (left part of the figures). Black circles in Figure 10d represent the depths of the 9 April 2001 aftershocks. T_m, the mechanical thickness deduced from the depth of the 800° C isotherm, is 45 km. T_l, the isotherm of the transition depth between semibrittle and ductile is at 34.5 km. The slab-pull force necessary to reach the rupture limit at the depth where occurred the main shock and 40% of the aftershocks is 0 (thick line), for 70%, it is 1.5×10^{12} N m^{-1} with an associated stress of 43 MPa (dashed thick line), and for 90% it is 4.4×104^{12} N m^{-1} with an associated stress of 403 MPa (dotted line).

Table 5. Stress and Dynamic Force Necessary to Change the Depth of the Brittle Limit Within the Mechanical Lithosphere[a]

Type	Depth, km	% Events	Stress, MPa	Force, N m^{-1}
Tensional	18	2001	0	0
	22	2001 + 40%	0	0
	25	2001 + 70%	35	1.2×10^{12}
	29	2001 + 90%	403	4.4×10^{12}
Compressional	27	1981 + 1982	600	1.4×10^{13}
	30	1981	370	10^{13}

[a]The numerals 2001, 1981, and 1982 mean the 2001, 1981, and 1982 earthquakes and the percentages are those of the aftershocks of the 2001 main event.

[31] The thermal stress (Figure 10a) for a lithosphere of age t, at depth z, is given by the formula proposed by *Wessel* [1992]

$$\sigma = \frac{T_m \alpha_l E}{(1-\nu)}\left[\frac{T_l}{T_m} - erf\left(\frac{z}{2\sqrt{\kappa t}}\right) - \frac{\lambda\beta}{A\sqrt{\pi}}\ln\left(\frac{z}{2A\sqrt{\kappa t}}\right)\right] \quad (8)$$

where α_l is the linear thermal expansion coefficient, T_l = 590°C is the temperature at the depth of the brittle-ductile transition (29.5 km in our case), *erf* is the error function, κ the thermal diffusivity, A and β constants ($A = erf^{-1}(T_l/T_m)$, $\beta = e^{-A2}-1$), and λ is a measure of how much the thermal contraction stresses have been relieved (we take λ = 0.8). The parameters used are the same as those proposed by *Wessel* [1992]. Indeed, the thermal stress has a minor influence on our YSE, as the bending stress at shallow depth overwhelms the thermal stress, and deeper, the thermal stress is low (Figure 10a).

[32] The plate bending stress (Figure 10b) follows the thermal stress, and is defined by m, the slope of the elastic core, related to K, the curvature of the bending by $m = KE/(1 - \nu^2)$. K is obtained from the wavelength x_b and the amplitude w_b of the bending [e.g., *McNutt*, 1984]

$$K(x=0) = -\sqrt{2}\pi^2 w_b e^{\frac{\pi}{4}}/8x_b^2 \quad (9)$$

[33] We find $K = -10.9 \times 10^{-7}$ m^{-1}.

[34] The in-plane stress (Figure 10c) is a constant that we adjust as a function of the depth of the 2001 main event and its aftershocks. Results will be discussed later in section 4.4. The computation method of the compound stresses is described in detail by *Mueller et al.* [1996a]. First, the thermal stress is applied, the stress distribution must be bounded by the yield envelope, and the stress integral must vanish as the in-plane force is zero. Second, a bending stress of the form $mz + b$ is added, with the same conditions that enable the determination of the constant b. Third, the in-plane stress is added, and this time, the stress integral is equal to the in-plane force.

4.4. Distribution of Stress Within the Lithosphere

[35] Our final distribution of stress within the lithosphere is shown in Figure 10d. It is derived from classical YSE theory, and only the in-plane stress parameter is adapted to our study. To avoid confusion between depth below sea level, which is the reference for the seismic events, and below the seafloor, which is the reference for the YSE, we will use depth below sea level in the following discussion.

[36] Because of the effect of the bending prior to subduction, the mechanical lithosphere is in tension in its upper part and the tensional stress reaches the YSE from the top of the crust to a depth of at least 22 km. This part of the lithosphere can experience tensional brittle failure. At intermediate depths, stresses are not sufficient to produce failure since this is the elastic core where deformation is elastic. Finally, down to 45 km, deformation induces creep flow in compression. The adjustment of the depth of the transition between brittle tensional and elastic behavior is related to the depth of the main event of 2001 and its aftershocks. If we only consider the 2001 event, no tensional force is needed to initiate brittle failure at 22 km depth, whereas if we want 70% of the aftershocks to fall within the brittle lithosphere, we need a tensional force of 1.5×10^{12} N m^{-1}, and if we want 90%, a force of 4.4×10^{12} N m^{-1} is required (see Table 5).

[37] We find tensional forces between 0 and 4.4 *times* 10^{12} N m^{-1}, depending on the chosen depth of the transition between brittle rupture and elastic behavior. This force corresponds to the slab-pull force transmitted on the other side of the interplate zone. Recent studies [*Bott*, 1993; *Schellart*, 2004; *Sandiford et al.*, 2005] indicate that it usually ranges between 10^{12} and 4×10^{12} N m^{-1}, decreasing with an increasing coupling coefficient. Central Chile has a high coupling coefficient (χ = 0.56 [*Scholz and Campos*, 1995]); thus the transmitted tensional force is probably close to zero when the subduction is locked. However, even when the subduction is unlocked, the effect of the flat subduction might reduce locally the transmission of the slab pull force. From laboratory experiments, [*Schellart*, 2004] showed that the ratio of transmission of the slab pull force decreases with the dip angle of the subduction plate and is 0–4% for dip angles between 15 and 30°. In central Chile, after 150 km of shallow dip subduction (15°), the Nazca plate presents a flat segment of about 300 km-length [*Gutscher et al.*, 2000]. Hence the transmission of the slab pull force is probably small in our study region. For these reasons, we think that the actual tensional force ranges between 0 and 10^{12} N m^{-1}. It is hard to be more precise since, in our analysis, we take into account the 2001 event aftershocks, whose depths are poorly constrained due to the asymmetrical location of the seismological network.

[38] From the 72 aftershocks studied, the three deepest are well separated from the main group and are from 42 to 46 km deep. Because of high pressure expected at these depths, brittle fracturing or frictional sliding on fault surfaces is prohibited. Some additional effects that reduce the strength of rocks are therefore required. Fluid released due to dehydration of hydrous minerals can increase pore pressure and promote brittle fracture. This dehydration embrittlement phenomenon is commonly used to explain intraplate intermediate depth seismicity, i.e., earthquakes with $z < 300$ km [*Kirby et al.*, 1996a]. It can occur if rocks have been hydrated prior to subduction and if they support stresses such as bending ones. Possible causes for rock hydrating are faulting or alteration and the magmatic effects of plumes [*Seno and Yamanaka*, 1996; *Green*, 2001; *Yamasaki and Seno*, 2003]. In our study area the 9 April 2001 event and its aftershocks are located below the O'Higgins fault and other horst-and-graben normal faults

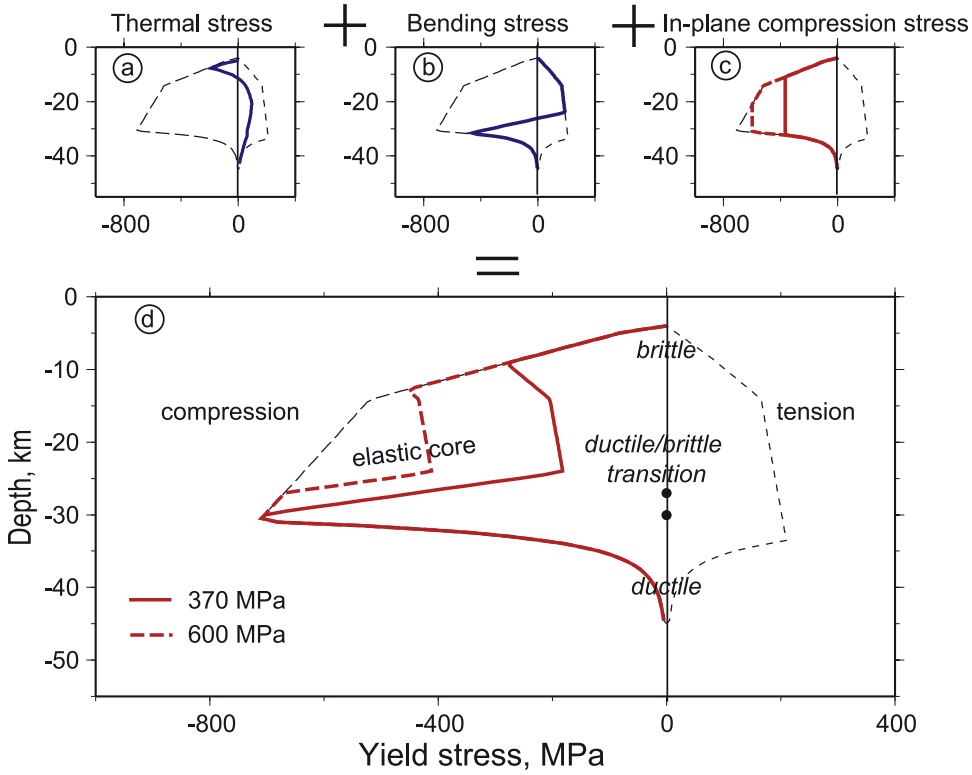

Figure 11. Yield strength envelope computed in the case of (a) pure thermal stress, (b) pure bending, and (c) pure compression, and (d) their sum with thermal and bending preceding compression. Black circles represent the 1981 and 1982 outer rise events at their published depth (30 and 27 km). The compressive force necessary to reach the rupture limit at 30 km depth is 10^{13} N m^{-1} (thick line). At 27 km, it is 1.4×10^{13} N m^{-1} (dashed line).

associated with the outer trench and along the JF hotspot ridge. Although horst-and-graben type faults are not usually assumed to extend very deep, the conjunction of the O'Higgins fault and the hotspot ridge might cause rock hydration at a depth that could explain these three deep aftershocks.

[39] The 9 April 2001 event and the remaining aftershocks are located in the brittle-ductile transition zone of the lithosphere, where both mechanisms are possible. According to the distribution of stresses deduced from the yield stress envelope, the elastic core of the lithosphere begins deeper than 22 km, and the neutral plane, defined as the depth where the lithosphere is neither in tension nor in compression, is roughly at a depth of 26 km (Figure 10d), whatever the chosen in-plane stress is. This shows that the empirical depth of the neutral plane proposed by *Seno and Yamanaka* [1996] at the 450°C isotherm (21 km + 4 km here) is appropriated in that case, but we will see that it is about 5 km deeper in compression (Figure 11).

5. Discussion

5.1. Temporal Evolution of the Outer Rise Stress

[40] The YSE of the lithosphere presented above is a snapshot of the state of stress of the lithosphere during the month of April 2001. With a reasonable value of the in-plane tension, it accounts for the vertical distribution of the outer rise seismicity. This YSE also demonstrates the impossibility of compressional events under these same conditions. However, the occurrence of 1981 and 1982 compressional events (see Table 1) in the same area implies that the lithosphere had at that time a compressive part at depth. Outer rise in-plane forces are directly related to the subduction processes associated with stress accumulation and release during the earthquake cycle. When the subduction is locked, the outer rise lithosphere is in compression [*Christensen and Ruff*, 1988; *Astiz et al.*, 1988; *Dmowska et al.*, 1988; *Lay et al.*, 1989], and when sliding, outer rise lithosphere can be in tension because of slab-pull [*Kanamori*, 1971; *Abe*, 1972].

[41] We construct a new YSE combining unchanged thermal and bending stresses, which correspond to the ambient stress regime associated to the static deformation as defined by *Lay et al.* [1989], this time followed by in-plane compression, which corresponds to the dynamical regional stress. As we did in section 4.3, the value of the in-plane force is chosen so that the two events should be located in an area where compressive failure can occur (Table 5). In this case, if we want compressional brittle failure to occur at 30 km or 27 km depth, we have to impose compressional forces of 10^{13} N and 1.4×10^{13} N, respectively, which correspond to in-plane compressional stresses of 370 MPa and 600 MPa (Figure 11). These force values are about 5 to 10 times greater than the tensional forces found for the 2001 period. It is due to the symmetrical distribution of the thermal and bending stresses with respect to the neutral plane and because the YSE is greater in compression than in tension, which results from the fact that the lithosphere is stronger in compression than in tension.

Thus a greater force is needed to initiate rupture in compression. Main dynamic forces acting in compression on the plate are the ridge push force, the resistive force, which comprises the buoyancy effect and the shearing force at the interface between the slab and the mantle, and the drag force. The resistive force has been estimated to be in the order of 7×10^{12} N by [*Wortel and Cloetingh*, 1985]. The drag force and the ridge-push force build up between two great interplate events. In our case, the Valparaíso 1906 earthquake [*Gutemberg and Richter*, 1954; *Okal*, 2005] was the last great earthquake before that of 1985 [*Korrat and Madariaga*, 1986; *Comte et al.*, 1986]. In the hypothesis of no or little sliding during the locked subduction, the force we calculate corresponds to the accumulation of stresses during 75 years.

[42] Hence we propose that the major interplate underthrust 1985 Mw = 7.8 Valparaíso earthquake sufficiently unlocked the subduction so that before, the oceanic lithosphere seaward of the trench was subject to a high level of in-plane compression force and, since the 1985 event, to an in-plane tension force. It can be noted from Table 1 that the 1982 earthquake was shallower than the 1981 event. Whatever the uncertainties in the depth determination might be, it is logical that the latter was shallower because the compressional stress increased with time. The outer rise compressive events of 1981 and 1982 are located 100 km seaward the 1985 Valparaíso event, in the direction of the plate convergence. The 2001 event was located at the same distance from the Valparaíso earthquake but shifted 50 km to the north from the axis of the convergence direction. It is within the area perturbed by the 1985 event [*Comte et al.*, 1986; *Mendoza et al.*, 1994] and also within the southern limit of the 1971 interplate earthquake [*Comte et al.*, 1986]. The addition of the effects of these two events could explain the tensional state of stress of this part of the oceanic lithosphere and the consequently high level of seismicity. According to this model of stress accumulation, the stress drop that followed the 1985 event was probably smaller than the difference between our determination of in-plane tension and compression stresses. However, the 1985 event is the last great underthrusting event in the area, and thus this analysis confirms the change in stress regime during the earthquake cycle before and after a major underthrust event.

5.2. Influence of the Juan Fernandez Ridge

[43] The seismic cycle that we outlined above shows a compressive period before 1985, followed by a still active tensional period but it does not explain the occurrence of 1971 outer rise tensional earthquake near the 9 April 2001 event. For this reason, we propose to take into account the effect of JF Ridge subducted seamounts (see location Figure 1). The high level of in-plane compression necessary to produce compressive outer rise earthquakes has been related to the stress accumulation induced by localized resistance to subduction [*Christensen and Ruff*, 1988] and is named the stress concentrator model [*Mueller et al.*, 1996b]. The mechanism involves subduction-zone asperities that present resistance to the subduction, which can be zones of strong coupling or loci of bathymetric irregularities subducting, both acting as stress concentrators. Coupling between plates occurs at asperities and large earthquakes occur when these asperities break [*Ruff*, 1992]. In our study area the deformation of San Antonio canyon has been attributed to the subduction of San Antonio seamount [*Laursen and Normark*, 2002], located between the Valparaíso underthrusting event and the 1981 and 1982 compressional outer rise earthquakes (Figure 1). The magnitude of an intraplate earthquake can be directly proportional to the size of an associated subducted seamount [*Cloos*, 1992], but in the case where the erosion of the margin is active, *Cloos* [1992] proposed that sediments can abort the failure associated with the subducted seamount. This could be a partial explanation for the difference between the northern study area, where events are mostly in tension, and the southern part. To the north, sediments are absent in the trench [*Flueh et al.*, 1998], and the beginning of the subduction of Papudo seamount [*Yáñez et al.*, 2001] is perhaps associated with erosion that limits the coupling and makes easier the occurrence of tensional outer rise events.

[44] Without the JF Ridge, the tensional stress field would be more important below the top of the bending. Outer rise earthquakes to the north of JF Ridge or to the south are indeed located in the bent area, close to the trench (Figure 2), whereas seismicity in our study area spreads out to the west of the bend in the direction of JF Ridge. This can be explained by the local increase in stress produced by the volcanic ridge. On the other hand, the occurrence of outer trench earthquakes depends not only on the regional stress accumulation, but also on preexisting weakness zones within the lithosphere. In our study area, horst-and-graben faults that usually characterize outer rise zone exist. Although their axis should be parallel to the trench, they strike parallel to the JF Ridge. The 1971 and 2001 event epicenters are located over these deep faults (Figure 1). Given our on-land local network, uncertainties in event locations in the east-west direction exist. However the fault plane of the 9 April 2001 main event is indeed subparallel to the strike of these crustal normal faults, and it is likely that this is also the case for the April 2001 aftershocks. In that case, the 9 April 2001 earthquake is evidence that the O'Higgins Fault probably affects the whole mechanical lithosphere. Finally, a reasonable explanation for the orientation of these normal faults and of the focal plane of the 9 April 2001 event is that the upper lithosphere is in extension because of bending prior to subduction, and the occurrence of the JF Ridge redirects the orientation of the horizontal tensional axis parallel to the ridge.

6. Conclusion

[45] The April 2001 outer rise tensional earthquake was caused by the bending of the lithosphere prior to subduction and an in-plane force associated with slab-pull. It is characterized by a strike of 41°, subparallel to the JF Ridge, a dip of 44°, and a rake of −84°. The source time function has a duration of 40 s, with a seismic moment of 4.6×10^{19} Nm. The depth of 12 km localizes this event below the Moho. This result, together with the depth distribution of the first 4 days of aftershocks indicates that the lithosphere is in tension down to a depth of 30 km.

[46] Our study outlines an important interaction between JF Ridge and the initiation of the subduction process at the trench. Outer rise events are shifted seaward from the

bending of the lithosphere where they should have occurred. The orientation of the tensional stress, as registered by the horst-and-graben fault direction and in the outer rise lithosphere, is shifted subparallel to the JF Ridge and it is likely that the O'Higgins fault acts on the whole mechanical lithosphere. It is interesting to note that the mechanism of the 9 April 2001 earthquake is also observed in other events down dip of the slab at about 100 km depth, probably indicating that these earthquakes occur by reactivation in preexisting structures formed at the initiation of the slab subduction at the trench. *Kirby et al.* [1996a, 1996b] indicated that faults produced at shallow depth in the trench outer rise setting (such as the JF chain off central Chile) being reactivated at greater depths may be useful for the assessment of seismic hazard of the region.

[47] The temporal evolution of the yield stress envelope of the oceanic lithosphere reveals a change in the in-plane stress regime from compression in the beginning of the 1980s to tension in 2001. This confirms the change in stress regime during the earthquake cycle before and after a major underthrust event, which in our case is the 1985 Mw 7.8 Valparáso earthquake. This seismic cycle might also be modulated by the presence of a subducted seamount, which can locally change the dynamic stress. Stresses necessary to explain the 2001 tensional failure range between 0 and 43 MPa, which indicate a slab-pull force acting on the oceanic lithosphere comprised between 0 and 1.5×10^{12} Nm^{-1}. It is in good agreement with recent estimations of the rate of transmission of the actual slab pull force in the mantle proposed by *Schellart* [2004] and by *Sandiford et al.* [2005]. Stresses necessary to explain the 1980's compressional events range between 370 and 600 MPa corresponding to a force of about 10^{13} Nm^{-1}, which results from the accumulation of stress since the last great interplate earthquake of 1906.

Appendix A: Velocity Model

[48] The unidimensional velocity model for Central Chile between latitudes 32°S and 35°S and longitude 74°W and 67°W is derived from the database of the Seismic catalogue from Seismological Service of Chile University (GUC). Among all the events recorded in the area between 01-01-2001 and 28-02-2003, we select only those corresponding to the following criteria: (1) registered by a minimum number of six stations, (2) root mean square (RMS) residual less than 0.3 s, (3) more than 10 readings of either P or S wave arrivals, and (3) depth error <10 km. On 1046 events, 1017 fulfill the former criteria. These events are located using the set of programs for analysis of data SEISAN [*Havskov and Ottemoller*, 1999]. Initial hypocenter locations obtained are used as input for program VELEST [*Kissling et al.*, 1995], which realizes a simultaneous inversion for hypocenters and velocity model. The final structure velocity model is that which minimizes the errors. Once the final velocity model is obtained and after the corresponding corrections in the readings of P and S phases, final hypocenter relocations (Figures 6 and 8) are carried out using VELEST.

[49] **Acknowledgments.** This a contribution to the FONDECYT program 1040808 and to the Millenium Science Nucleus of Seismotectonics and Seismic Hazard P02-033-F. AL was supported from an CONICYT/ECOS grant funded by the French Ministry of Research and by the government of Chile. Most of the figures were drawn using GMT public software [*Wessel and Smith*, 1995]. The authors thank Wouter Schellart, Sierd Cloetingh, and an anonymous reviewer for thoughtful reviews and Mark Falvey for comments on the English. International Associated Laboratory Montessus de Ballore CNRS-IPGP-ENS/U. de Chile contribution LIA-MB01.

References

Abe, K. (1972), Lithospheric normal faulting beneath the Aleutian trench, *Phys. Earth Planet. Inter.*, *5*, 190–198.
Astiz, L., T. Lay, and H. Kanamori (1988), Large intermediate depth earthquakes and the subduction process, *Phys. Earth Planet. Inter.*, *53*, 80–166.
Barazangi, M., and B. Isacks (1976), Spatial distribution of earthquakes and subduction of the Nazca Plate beneath South America, *Geophysics*, *4*, 686–692.
Bijwaard, H., W. Spakman, and E. Engdahl (1998), Closing the gap between regional and global travel time tomography, *J. Geophys. Res.*, *103*, 55–78.
Bodine, J., M. Stekler, and A. Watts (1981), Observations of flexure and the rheology of the oceanic lithosphere, *J. Geophys. Res.*, *86*, 3695–3707.
Bott, M. H. P. (1993), Modelling the plate-driving mechanism, *J. Geol. Soc. London*, *150*, 941–951.
Brace, W., and D. Kohlstedt (1980), Limits on lithospheric stress imposed by laboratory experiments, *J. Geophys. Res.*, *85*, 6248–6252.
Byerlee, J. (1978), Friction of rocks, *Pure Appl. Geophys.*, *116*, 615–626.
Caldwell, J., W. Haxby, D. Karig, and D. Turcotte (1976), On the applicability of a universal elastic trench profile, *Earth Planet. Sci. Lett.*, *31*, 239–246.
Campos, J., R. Madariaga, J. Nábělek, B. Bukchin, and A. Deschamp (1994), Faulting process of the 1990 June 20 Iran earthquake from broad-band records, *Geophys. J. Int.*, *118*, 31–46.
Cande, S., and E. Herron (1982), The early Cenozoic history of the southeast Pacific, *Geophys. Res. Lett.*, *57*, 63–74.
Chapple, W., and D. Forsyth (1979), Earthquakes and bending of plates at trenches, *J. Geophys. Res.*, *84*, 6729–6749.
Chopra, P., and M. Paterson (1981), The experimental deformation of dunite, *Tectonophysics*, *78*, 453–473.
Christensen, D., and L. Ruff (1983), Outer-rise earthquakes and seismic coupling, *Geophys. Res. Lett.*, *10*, 697–700.
Christensen, D., and L. Ruff (1988), Seismic coupling and outer rise earthquakes, *J. Geophys. Res.*, *93*, 13,421–13,444.
Cloos, M. (1992), Thrust-type subduction zone earthquakes and seamount asperities: A physical model for seismic rupture, *Geology*, *20*, 601–604.
Clouard, V., R. Zapata, and E. Vera (2003), Modal depth analysis of the oceanic lithospheric bending along the Chilean margin, from a new detailed bathymetric synthesis, in, *Eos Trans. AGU*, *84*(46), Fall Meet. Suppl., Abstract S41D-0119.
Comte, D., A. Eisenberg, E. Lorca, M. Pardo, L. Ponce, R. Saragoni, S. Singh, and G. Suarez (1986), The 1985 central Chile earthquake: A repeat of previous great earthquakes in the region, *Science*, *233*, 449–453.
DeMets, C., R. Gordon, D. Argus, and S. Stein (1990), Current plate motions, *Geophys. J. Int.*, *101*, 425–478.
Dmowska, R., and L. Lovison (1988), Intermediate-term seismic precursors for some coupled subduction zones, *Pure Appl. Geophys.*, *126*, 643–664.
Dmowska, R., and L. Lovison (1992), Influence of asperities along subduction interfaces on the stressing and seismicity of adjacent areas, *Tectonophysics*, *211*, 23–43.
Dmowska, R., J. Rice, L. Lovison, and D. Josell (1988), Stress transfer and seismic phenomena in coupled subduction zones during the earthquake cycle, *J. Geophys. Res.*, *93*, 7869–7884.
Dmowska, R., G. Zheng, and J. Rice (1996), Seismicity and deformation at convergent margins due to heterogeneous coupling, *J. Geophys. Res.*, *101*, 3015–3029.
Engdahl, E., R. van der Hilst, and R. Buland (1998), Global teleseismic earthquake relocation with improved travel time and procedures for depth relocation, *Bull. Seismol. Soc. Am.*, *88*, 722–743.
Flueh, E., et al. (1998), Seismic investigation of the continental margin off- and onshore Valparaiso, Chile, *Tectonophysics*, *288*, 251–263.
Goetze, C. (1978), The mechanism of creep in olivine, *Phil. Trans. R. Soc. London, Ser. A*, *288*, 99–119.
Goetze, C., and B. Evans (1979), Stress and temperature in the bending lithosphere as constrained by experimental rock mechanics, *Geophys. J. R. Astron. Soc.*, *59*, 463–478.
Green, H. W. (2001), Physical mechanisms for earthquakes at intermediate depths, *Eos Trans. AGU*, *82*(47), Fall Meet. Suppl., Abstract S42D-03.
Gutemberg, B., and C. Richter (1954), *Seismicity of the Earth*, 310 pp., Princeton Univ. Press, Princeton, N. J.

Gutscher, M.-A. (2002), Andean subduction styles and their effect on thermal structure and interplate coupling, *J. South Am. Earth Sci.*, *15*, 3–10.
Gutscher, M., W. Spakman, H. Bijwaard, and E. Engdhal (2000), Geodynamics of flat subduction: seismicity and tomographic constraints from the Andean margin, *Tectonics*, *19*, 814–833.
Hasegawa, A., and I. Sacks (1981), Subduction of the Nazca Plate beneath Peru as determined by seismic observations, *J. Geophys. Res.*, *86*, 4971–4980.
Havskov, J., and L. Ottemoller (1999), *SEISAN: The Earthquakes Analysis Software*, Inst. of Solid Earth Phys., Univ. of Bergen, Bergen, Norway.
Judge, A., and M. McNutt (1991), The relationship between plate curvature and elastic plate thickness: A study of the Peru-Chile Trench, *J. Geophys. Res.*, *96*, 16,625–16,639.
Kanamori, H. (1971), Seismological evidence for a lithospheric normal faulting—The Sanriku earthquake of 1933, *Phys. Earth Planet. Inter.*, *4*, 289–300.
Kendrick, E., M. Bevis, R. Smalley, B. Brooks, R. Vargas, E. Lauria, and L. Fortes (2003), The Nazca-South America Euler vector and its rate of change, *J. South Am. Earth Sci.*, *16*, 125–131.
Kirby, S. (1980), Tectonic stresses in the lithosphere: Constraints provided by the experimental deformation of rocks, *J. Geophys. Res.*, *85*, 6353–6363.
Kirby, S., E. Engdahl, and R. Denlinger (1996a), Intermediate-depth intraslab earthquakes and arc volcanism as physical expressions of crustal and uppermost mantle metamorphism in subducting slabs, in *Subduction: Top to Bottom*, *Geophys. Monogr. Ser.*, vol. 96, edited by G. Bebout et al., pp. 195–214, AGU, Washington, D. C.
Kirby, S., E. Engdahl, and E. Okal (1996b), The Juan Fernandez earthquake zone of central Chile and Argentina at 34 to 30.5°S: Fine structure and evidence of reactivation of shallow intraplate faults at intermediate depths, in, *Eos Trans. AGU*, *77*(17), Spring Meet. Suppl., Abstract S275.
Kissling, E., U. Kradolfer, and H. Maurer (1995), *Program VELEST Users Guide-Short Introduction*, Inst. of Geophys. and Swiss Seismol. Serv., Zurich, Switzerland.
Kohlstedt, D., B. Evans, and S. Mackwell (1995), Strength of the lithospheric: Constraints imposed by laboratory experiments, *J. Geophys. Res.*, *100*, 17,587–17,602.
Kopp, H., E. Flueh, C. Papenberg, and D. Klaeschen (2004), Seismic investigations of the O'Higgins Seamount Group and Juan Fernández Ridge: Aseismic ridge emplacement and lithosphere hydration, *Tectonics*, *23*, TC2009, doi:10.1029/2003TC001590.
Korrat, I., and R. Madariaga (1986), Rupture of the Valparaiso (Chile) gap from 1971 to 1985, in *Earthquake Source Mechanics*, *Maurice Ewing Ser.*, vol. 6, edited by S. Das, J. Boatwright, and C. Scholz, pp. 247–258, AGU, Washington, D. C.
Laursen, J., and W. Normark (2002), Late Quaternary evolution of the San Antonio Submarine Canyon in the central Chile forearc (33°S), *Mar. Geol.*, *188*, 365–390.
Lawrie, A., and R. Hey (1981), Geological and geophysical variations along the western margin of Chile near lat 33° to 36°S and their relation to Nazca plate subduction, in *Nazca Plate: Crustal Formation and Andean Convergence*, edited by L. Kulm et al., Mem. Geol. Soc. Am., *154*, 741–754.
Lay, T., L. Astiz, H. Kanamori, and D. Christensen (1989), Temporal variation of large interplate earthquakes in coupled subduction zones, *Phys. Earth Planet. Inter.*, *54*, 258–312.
Levitt, D., and D. Sandwell (1995), Lithospheric bending at subduction zones based upon depth soundings and satellite gravity, *J. Geophys. Res.*, *100*, 379–400.
Malgrange, M., A. Deschamps, and R. Madariaga (1981), Thrust and extensional faulting under the Chilean coast: 1965, 1971 Aconcagua earthquakes, *Geophys. J. R. Astron. Soc.*, *66*, 313–331.
McNutt, M. (1984), Lithospheric flexure and thermal anomalies, *J. Geophys. Res.*, *89*, 11,180–11,194.
McNutt, M., and H. Menard (1982), Constraints on the yield strength in the oceanic lithosphere derived from observations of flexure, *Geophys. J. R. Astron. Soc.*, *71*, 363–394.
Mendoza, C., S. Hartzell, and T. Monfret (1994), Wide-band analysis of the 3 March 1985 central Chile earthquake: Overall source process and rupture history, *Bull. Seismol. Soc. Am.*, *84*, 269–283.
Mueller, S., G. Choy, and W. Spence (1996a), Inelastic models of lithospheric stress - I. Theory and application to outer rise plate deformation, *Geophys. J. Int.*, *125*, 39–53.
Mueller, S., W. Spence, and G. Choy (1996b), Inelastic models of lithospheric stress - II. Implications for outer rise seismicity and dynamics, *Geophys. J. Int.*, *125*, 54–72.
Müller, D., W. Roest, J. Royer, L. Gahagan, and J. Sclater (1996), Age of the ocean floor, *Rep. MGG-12*, World Data Cent. for Mar. Geol. and Geophys., Boulder, Colo.
Nábělek, J. (1984), Determination of earthquake source parameters from inversion of body waves, Ph.D. thesis, Mass. Inst. of Technol., Cambridge, Mass.
Okal, E. (2005), A re-evaluation of the great Aleutian and Chilean earthquakes of 1906 August 17, *Geophys. J. Int.*, *161*, 268–282.
Pardo, M., D. Comte, and T. Monfret (2002), Seismotectonic and stress distribution in the central Chile subduction zone, *J. South Am. Earth Sci.*, *15*, 11–22.
Parsons, B., and J. Sclater (1977), An analysis of the variation of the ocean floor bathymetry and heat flow with age, *J. Geophys. Res.*, *82*, 803–827.
Renkin, M., and J. Sclater (1988), Depth and age in the north Pacific, *J. Geophys. Res.*, *93*, 2919–2935.
Ruff, L. (1992), Asperity distributions and large earthquake occurrence in subduction zones, *Tectonophysics*, *211*, 61–83.
Sandiford, M., D. Coblentz, and W. P. Schellart (2005), Evaluating slab-plate coupling in the Indo-Australian plate, *Geology*, *33*, 113–116.
Schellart, W. P. (2004), Quantifying the net slab pull force as a driving mechanism for plate tectonics, *Geophys. Res. Lett.*, *31*, L07611, doi:10.1029/2004GL019528.
Scholz, C. (2002), *The Mechanics of Earthquakes and Faulting*, 2nd ed., 471 pp., Cambridge Univ. Press, New York.
Scholz, C., and J. Campos (1995), On the mechanism of seismic decoupling and back arc spreading at subduction zones, *J. Geophys. Res.*, *100*, 22,103–22,115.
Seno, T., and D. Gonzalez (1987), Faulting caused by earthquakes beneath the outer slope of the Japan Trench, *J. Phys. Earth*, *35*, 381–407.
Seno, T., and Y. Yamanaka (1996), Double seismic zones, compressional deep trench-outer rise events and superplumes, in *Subduction: Top to Bottom*, *Geophys. Monogr. Ser.*, vol. 96, edited by G. Bebout et al., pp. 347–355, AGU, Washington, D. C.
Stauder, W. (1968a), Mechanism of the Rat Island earthquake sequence of February 4, 1965 with relation to island arcs and see-floor spreading, *J. Geophys. Res.*, *73*, 3847–3858.
Stauder, W. (1968b), Tensional character of earthquake foci beneath the Aleutian Trench with relation to sea-floor spreading, *J. Geophys. Res.*, *73*, 7693–7701.
Taylor, M. A., G. Zheng, J. Rice, W. Stuart, and R. Dmowska (1996), Cyclic stressing and seismicity at strongly coupled subduction zones, *J. Geophys. Res.*, *101*, 8363–8381.
Turcotte, D., and G. Schubert (1982), *Geodynamics-Applications of Continuum Physics to Geological Problems*, John Wiley, Hoboken, N. J.
von Huene, R., J. Corvalan, E. Flueh, K. Hinz, J. Korstgard, C. Ranero, W. Weinrebe, and the CONDOR Scientists (1997), Tectonic control of the subducting Juan Fernandez Ridge on the Andean margin near Valparaiso, Chile, *Tectonics*, *16*, 474–488.
Waldhauser, F. (2001), HypoDD: A program to compute double-difference hypocenter locations, *Open File Rep. 01-113*, U.S. Geol. Surv., Reston, Va.
Watts, A., J. Cochran, and G. Selzer (1975), Gravity anomalies and flexure of the lithosphere: A three-dimensional study of the Great Meteor Seamount, northeast Atlantic, *J. Geophys. Res.*, *80*, 1391–1398.
Watts, A., S. Lamb, J. Fairhead, and J. Dewey (1995), Lithospheric flexure and bending of the Central Andes, *Earth Planet. Sci. Lett.*, *134*, 9–21.
Wessel, P. (1992), Thermal stress and the bimodal distribution of elastic thickness estimates of the oceanic lithosphere, *J. Geophys. Res.*, *97*, 14,177–14,193.
Wessel, P., and W. Smith (1995), *The GMT-SYSTEM, Technical Reference Cookbook*, School of Ocean Earth Sci. and Technol., Univ. of Hawaii at Manoa, Manoa, Hawaii.
Wortel, M., and S. Cloetingh (1985), Accretion and lateral variations in tectonic structure along the Peru-Chile Trench, *Tectonophysics*, *112*, 443–462.
Yamasaki, T., and T. Seno (2003), Double seismic zone and dehydration embrittlement of the subducting slab, *J. Geophys. Res.*, *108*(B4), 2212, doi:10.1029/2002JB001918.
Yáñez, G., C. Ranero, R. von Huene, and J. Diaz (2001), Magnetic anomaly interpretation across the southern central Andes (32°–34°S): The role of the Juan Fernandez Ridge in the late Tertiary evolution of the margin, *J. Geophys. Res.*, *106*, 6325–6345.
Zapata, R. (2001), Estudio batimetrico del margen chileno, Master's thesis, Univ. de Chile, Santiago, Chile.

J. Campos, V. Clouard, E. Kausel, and A. Perez, Departamento de Geofísica, Universidad de Chile, Blanco Encalada 2002, 8370449 Santiago, Chile. (valerie@dgf.uchile.cl)

A. Lemoine, Development Planning and Natural Risks Division, Bureau de Recherches Géologiques et Miniéres, 3 Avenue Claude-Guillemin, BP 36009, F-45060 Orléans Cedex 2, France.